Early identification and tracking of fragments from break-up events

Alejandro Pastor
GMV, apastor@gmv.com
Jan Siminski
Space Debris Office, jan.siminski@esa.int
Guillermo Escribano
University Carlos III of Madrid, guescrib@ing.uc3m.es
Manuel Sanjurjo-Rivo
University Carlos III of Madrid, manuel.sanjurjo@uc3m.es
Diego Escobar
GMV, descobar@gmv.com

Abstract

Break-up events represent the dominant source of objects in space catalogues, surpassing half of the overall population. These not so uncommon events include explosions, collisions or anomalous events resulting in fragmentations and their number is estimated to be higher than 630. Two of the most massive events, involving a number of fragments in the order of few thousands are the Fengyun 1C Anti-Satellite (ASAT) test in 2007 and the accidental collision of Cosmos 2251 and Iridium 33 in 2009, accounting for over 30% of all catalogued space objects. In 2021, three main break-up events happened: the failure of NOAA 17 (10th March), an accidental collision of YunHai 1-02 with a small mission-related debris object (18th March) and the destruction of Cosmos 1408 in an ASAT test (15th November). As of today, the number of catalogued fragments by the 18th Space Defense Squadron (SDS) associated to these events is 115 (1 decayed), 37 (4 decayed) and 1561 (243 decayed), respectively.

The early detection and cataloguing of the fragments generated during these events poses a complex challenge for space objects catalogue build-up and maintenance processes. These fragments are first part of a dense cloud of debris, which spreads over time, making the identification of individual objects rather difficult in the early stages. Hence, a trade-off between cataloguing time and reliability arises, where time favours the spreading of the objects along the orbit, thus reducing the probability of false associations and the uncertainty of the estimated trajectories, since more data is available. However, the provision of Space Situational Awareness products and services during the few first days after a break-up event can be crucial to avoid collisions between the fragments and other space objects, particularly in highly congested regimes, such as Low Earth Orbit. In this regard, reducing the time required to accurately estimate the trajectories of the fragments may enable the execution of collision avoidance manoeuvres, in the case of operational space objects with manoeuvre capabilities, and analyse potential collision cascade events, which may endanger the space environment.

This paper studies the whole cataloguing process after a break-up event, starting from a catalogue with no fragments from the fragmentation under-analysis, and until a well-established orbit is obtained for all the fragments, using a ground-based sensor network. First, the observations enter a multi-sensor multi-target track-to-track association algorithm in charge of grouping observations belonging to the same objects. To resolve the ambiguity, particularly shortly after the event, hypotheses about tracks belonging to the same fragment are generated, scored, pruned, and promoted, only when there is enough confidence, leading to the initialisation of new objects in the catalogue. As soon as the catalogue is populated, a track-to-orbit correlation algorithm is responsible for the correlation of observations and already catalogued orbits. This alleviates the track-to-track association and enables the update of the orbital estimates, required for maintaining the catalogue.

1. INTRODUCTION

The 18th Space Defense Squadron (SDS) maintains one of the most complete and publicly available catalogues of space objects. It is published on Space-Track [1] and contains around 25,000 objects currently orbiting the Earth, of which more than half are classified as fragmentation debris. Break-up events represent the dominant source of objects in space catalogues. The first known accidental break-up happened in 1961 (Able Star upper stage explosion after separation from Transit 4-A)and generated a number of trackable objects more than three times greater than the number of known satellite population at that time. Table 1 presents the ten most relevant break-up events in terms of number of catalogued fragments.

Table 1: Ten most relevant break-up events in terms of number of catalogued fragments. Recent Cosmos 1408 data retrieved from [2, 1], historic data gathered from [3].

#	Object	Date	Number of fragments		Apogee	Perigee	Inclination	Cause
			Cataloged	On-orbit	(km)	(km)	(deg)	
1	FENGYUN 1C (1999-025A)	11-Jan-07	3442	2832	865	845	98.6	Delib. coll.
2	COSMOS 1408 (1982-092A)	15-Nov-21	1700	729	490	465	82.6	Delib. coll.
3	COSMOS 2251 (1993-036A)	10-Feb-09	1668	1076	800	775	74	Accid. coll.
4	IRIDIUM 33 (1997-051C)	10-Feb-09	628	333	780	775	86.4	Accid. coll.
5	STEP II R/B (1994-029B)	03-Jun-96	754	82	820	585	82	Propulsion
6	IRIDIUM 33 (1997-051C)	10-Feb-09	628	333	780	775	86.4	Accid. coll.
7	COSMOS 2421 (2006-026A)	14-Mar-08	509	0	420	400	65	Unknown
8	SPOT 1 R/B (1986-019C)	13-Nov-86	498	31	835	805	98.7	Propulsion
9	COSMOS 1275 (1981-053A)	24-Jul-81	479	421	1015	960	83	Battery
10	OV2-1/LCS 2 R/B (1965-082DM)	15-Oct-65	473	32	790	710	32.2	Propulsion

In-orbit fragmentations have been the most dominant source of space debris in the millimetre to decimetre size range. This is particularly critical for space safety, since objects in the upper part of this size range (centimetre to decimetre) are associated to the highest risk, given the current limits of shielding technology [4]. 18th SDS can currently track objects around 10 cm in low orbits and 1 m in Geostationary Earth Orbit (GEO), although these thresholds are expected to fall in the coming years due to the improvement in the Space Surveillance and Tracking (SST) sensor technology [5]. The number of debris objects greater than 10 cm estimated based on statistical models to be in orbit is around 36,500 [6]. However, when considering the range between 1 and 10 cm size, the population multiplies by almost a factor of 30 [6]. Thus we expect an important increase in complexity of catalogue build-up and maintenance activities in the coming years due to the higher number of observed objects.

The early detection and cataloguing of the fragments generated during these irregular events, around ten per year on average over the last decades [6], poses a complex challenge for space objects catalogue build-up and maintenance activities. Fragments behave as a dense cloud of debris, making the identification of individual objects difficult in the early stages. Time favours the spreading of the objects along the orbit, thus reducing the probability of false associations and the uncertainty of the estimated trajectories. The evolution of the cataloguing process of the fragments from Cosmos 1408 is a clear example of this complexity: 188 fragments detected and catalogued two weeks after the event (1st December), 715 the next month (903 total as of 1st January) and 499 the month following that (1402 total as of 1st February) [1]. Figure 1 shows the number of fragments for which Two Line Element (TLE) data was published on Space-Track [1], as well as the number of those reentered according to [2]. The first TLE from the fragmentation was published on 30th November, i.e., 15 days after the break-up. Since most operators and Space Situational Awareness (SSA) and Space Traffic Management (STM) operation centres rely on the 18th SDS Special Perturbations (SP) catalogue for their daily operations, this could have entailed a two weeks period with an incomplete population of objects, thus jeopardising the safety and sustainability of the Low Earth Orbit (LEO) environment. Note that the cataloguing date of each fragment is assumed to be the epoch of the first published TLE.

National Aeronautics and Space Administration (NASA) has been publishing a report on the history of on-orbit satellite fragmentations since 1984. The 15th edition [3], the most recent one, was published in 2018 and includes very valuable data about satellite break-ups up to 4 July 2018. Figure 2 shows the number of catalogued orbits and fragments still in-orbit from identified satellite break-up events in [3]. The two most recent peaks correspond to the

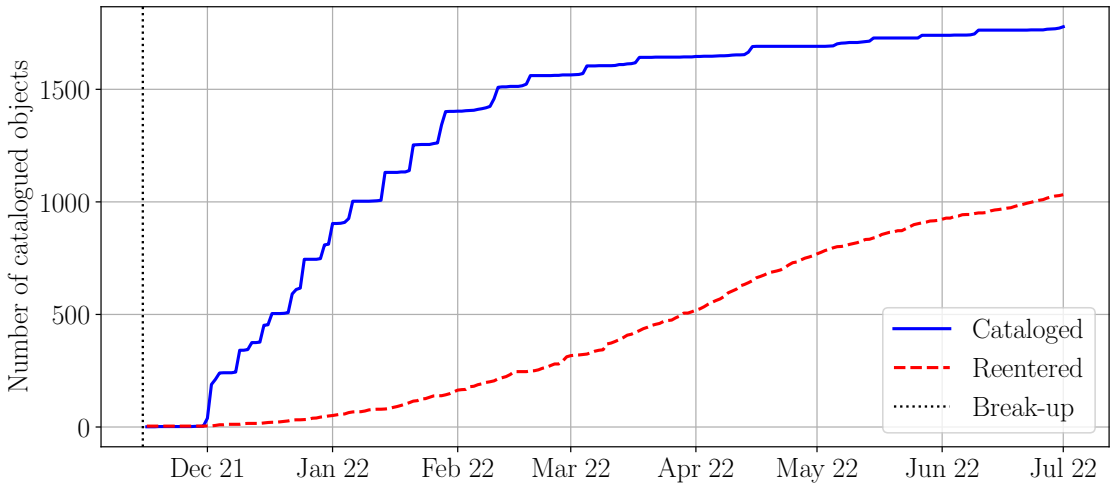

Figure 1: Cosmos 1408 Anti-Satellite (ASAT)-related objects catalogued by Space-Track [1].

Fengyun-1C Anti-Satellite (ASAT) test (2007) and the COSMOS 2251 and Iridium 33 collision (2009). Note that the report was published before the recent Cosmos 1408 ASAT test, so it is not included in the data set.

There are two main problems related to fragmentation events: 1) the detection of the fragments and first estimation of the orbits using observations from SST sensors and 2) the analysis of the fragmentation event using orbital data. This paper tackles the first problem and leaves the second one for future works.

Regarding the first problem, Crowther et al. [7] analyse a fragmentation of a Highly Elliptical Orbit (HEO) satellite after a collision with a LEO one. This scenario is considered a catastrophic break-up given the long orbital lifetime of HEO Resident Space Objects (RSOs) and their high relative velocity in LEO. This work suggests that the detection of fragments with ground-based optical sensors should favour observations at high altitude, since although the fragments are not as bright as at low altitude, the observation time is longer and the angular velocity lower. Johnson [8] investigates the break-up of the STEP M2 HAPS upper-stage in 1997, the worst fragmentation in terms of number of catalogued RSOs at that time. One day after the event, 120 fragments were detected and the 18th SDS catalogued 47 of them by the third day, 100 by the fourth day and 577 by the next month. Anselmo and Pardini [9] simulated six fragmentation events in GEO: a satellite in the GEO ring, two near-synchronous Titan Transtages and three Ariane IV third stages. Their simulated events include between 200 and 700 fragments greater than 10 cm.

The problematic of both large and small mean motion spreading of the fragments has been discussed by Saunders

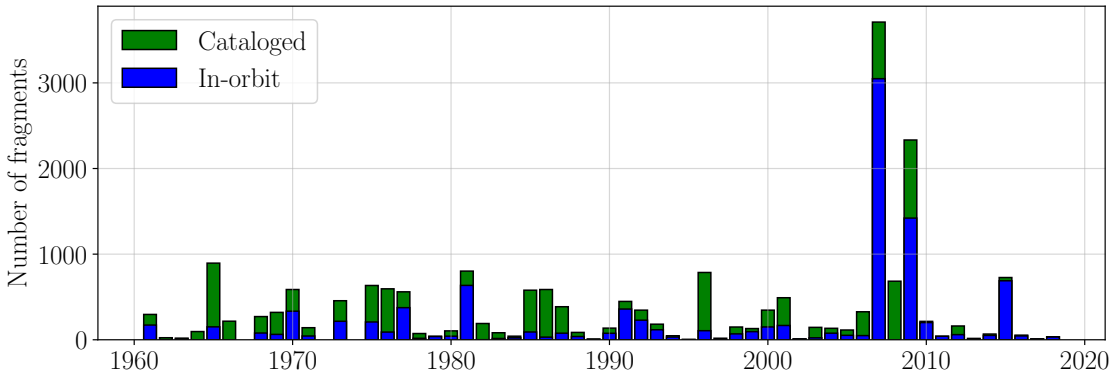

Figure 2: Number of catalogued (green) and in-orbit (blue) fragments from identified satellite break-up events per year according to [3] (from 1961 to 2018).

[10] and Schildknecht at al. [11], respectively. The first [10], elaborates on the observability conditions of a GEO fragmentation event. A satellite break-up is simulated using NASA breakup model [12] and considering 95 fragments of which only eight fragments are detected by a simulated survey network of three telescopes operating 45 days. The authors point that this low detection rate is caused by the large mean motion spreading of the fragments. The second [11], discusses the fragmentation events of the Titan 3C Transtage (#3692) in GEO and Atlas Centaur upper stage (#40209) in HEO during 2018, as well as two events related to Atlas Centaur upper stages (#35816 and #43652) in HEO during 2019. The number of fragments detected was more than 150 and 590 for the events of 2018 and more than 250 for those of 2019. Besides, the problematic of low mean motion dispersion is also discussed and tackled by means of an along-track survey strategy.

The suitability of Multiple Hypothesis Tracking (MHT) methods in cataloguing environments involving break-up events was confirmed by Singh et al. [13]. In this publication, one of the few presenting an operational-like scenario, several LEO satellite break-up events of increasing magnitude, involving up to 512 orbits and five radar sensors, are presented. Additionally, survey and tracking strategies must be optimised to maximise the number of detections and minimise the number of lost fragments [14]. Besides, magnitude measurements have been also used to identify fragments from a common break-up event [15].

The second problem, this is, the analysis of the fragmentation event using orbital data, involves the availability of orbits from the fragments, so it is usually tackled using TLEs. Johnson et al. [16] analyse the consequences of Fengyun-1C anti-satellite test, which again constituted the worst fragmentation event at the time. The special characteristics of the fragmentation lead to more than 2,000 fragments of 10 cm or greater size, most with a long orbital life, jeopardising space activities in LEO. One week after this intentional break-up event more than 600 fragments had been identified, although only 32 TLEs were published. The main cause of this disparity was the challenging radar observation correlation. Six months after the event 1967 fragments had been catalogued. Tetreault et al. [17] present a fragmentation event identification method based on TLEs. Identification of the location and time is shown to be greatly affected by the area-to-mass ratio of the debris object, yet a proper debris to parent RSO association is feasible with the proposed technique. Muciaccia [18] conducts a thorough study on the characteristics of LEO fragmentations. Based on TLE data, i.e. catalogued objects, a method is developed to characterise the fragmentation event in terms of the blast point, the debris generated and the parent body. Ephemerides from the JSC Vimpel catalogue [19] have also been successfully used for a posteriori analyses [20]. When available, the uncertainty in the orbits can be used to improve the fragmentation characterisation. In this regard, Faber et al. [21] compare different methods for the calculation of the blast point based on catalogued fragments. A statistical approach is conducted, so that there is uncertainty in the state of the fragments. The impact of the number of fragments, the fragmentation epoch and the level of uncertainty in the fragment Probability Distribution Functions (PDFs) on the computation of the blast point is analysed.

Moreover, particular orbit similarity metrics have been conceived for the correlation of catalogued debris fragments and parent bodies. Dimare et al. [22] propose an approach to correlate catalogued debris objects with their corresponding parent bodies. In this regard, the authors explore different orbit similarity metrics and analyse their applicability to the particular problem of break up time determination and parent identification.

The problem of early identification and tracking of fragments from break-up events is typically not studied from an operational perspective, undoubtedly due to the lack of publicly available data during the first days or even weeks after the events. To overcome this, we propose a simulated break-up scenario inspired on the recent Cosmos 1408 ASAT test with which study the whole cataloguing process just after the fragmentation. This paper covers the complete process starting with an empty catalogue, from the detection and first orbit estimation of the fragments (catalogue build-up) to the update of the initialised orbits with observations (catalogue maintenance). The methodology aims at reducing the blackout time after break-up events, so that the catalogue can accurately characterise the fragmentation debris as soon as possible.

This paper is organised as follows. In Section 2, we present the break-up simulation, observation simulation and cataloguing process. In Section 3, we provide and discuss the results obtained from evaluating the performance of the cataloguing process, including track-to-track association and track-to-orbit correlation, during the build-up and maintenance of the catalogue. Finally, in Section 4, we summarise and discuss the conclusions and future work of this preliminary study.

2. METHODOLOGY

The main elements of the methodology are depicted in Figure 3. First, the orbit of the parent object is used to simulate the break-up event and obtain the orbits of the fragments (Section 2.1). Secondly, observations, packed as tracks, for a sensor network are generated (Section 2.2). Thirdly, the cataloguing process builds and maintains a catalogue of fragments using these tracks as uncorrelated tracks (UCTs), i.e., the object they belong to is assumed to be unknown (Section 2.3). Finally, the estimation of the fragmentation epoch and its use to detect false positives as outliers is tackled (Section 2.4).

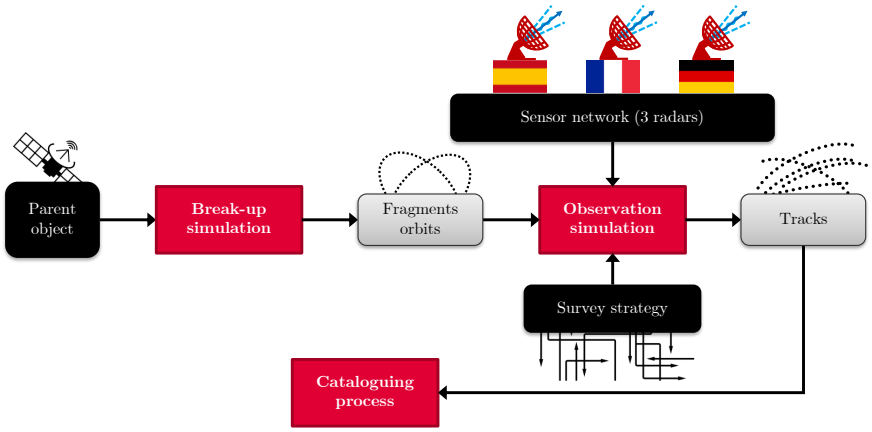

Figure 3: Main elements of the methodology.

2.1 Break-up simulation

Given the unavailability of public observation data regarding most of the break-up events just after the fragmentation, two approaches have been considered. Available TLE data was used to characterise a distribution of fragments (Section 2.1.1). Additionally, to confirm the completeness of this population of fragments, it has been compared against the one given by the NASA Standard Breakup Model (SBM) (Section 2.1.2).

2.1.1 TLE data

The fragments from the Cosmos 1408 ASAT test were first identified in CelesTrak's Satellite Catalogue (SATCAT) [2] as those with "OBJECT_NAME" field equal to "COSMOS 1408 DEB", a total of 1,778. Then, TLEs from these objects were downloaded from SpaceTrack [1].

The fragmentation can be modelled as an impulsive velocity increase, $\Delta\mathbf{v}$, added to the state of the parent object, Cosmos 1408, before the ASAT test. The position and velocity of the parent object at the fragmentation epoch, t_F, are $\mathbf{r}_{PF}$ and $\mathbf{v}_{PF}$, respectively. They can be obtained via orbit fitting with a high fidelity dynamical model on the last available TLEs before the fragmentation and represent the pinch point of the debris cloud. In the case under study, Cosmos 1408 ASAT test, $t_F = 2021\text{-}11\text{-}15\text{T}02{:}48$ [23, 24, 25] and the resulting state of the parent in Geocentric Celestial Reference Frame (GCRF) is

$$\begin{aligned} \mathbf{r}_{PF} &= \mathbf{r}_P\left(t = t_F\right) = \left[-1879.015,\, 1348.994,\, 6435.589\right]^T km \\ \mathbf{v}_{PF} &= \mathbf{v}_P\left(t = t_F\right) = \left[3.727686,\, 3.727686,\, 2.380025\right]^T km/s. \end{aligned} \tag{1}$$

For each fragment, an estimation process is triggered with the following set of estimated parameters:

$$\mathbf{y} = \left[\Delta\mathbf{v},\, B^\star\right]^T, \tag{2}$$

where $\Delta\mathbf{v} = \mathbf{v}(t = t_F) - \mathbf{v}_{PF}$ is the velocity increase of each fragment and $B^\star$ is the ballistic coefficient term of Simplified General Perturbations-4 (SGP4), which is convenient to collect model errors [26]. The actual observations are

$$\mathbf{z} = [\mathbf{r}_1, \ldots, \mathbf{r}_j, \ldots, \mathbf{r}_N]^T, \tag{3}$$

being $\mathbf{r}_j$ the position vector corresponding to the j^{th} TLE (at its epoch) from the N available TLEs of the fragment. The predicted observations are obtained by propagating the fragment state, given by $\mathbf{r}_{PF}$, $\mathbf{v}_{PF}$ and $\hat{\mathbf{y}}$, with SGP4 forward to the TLEs epochs, i.e.,

$$\hat{\mathbf{z}}(t) = \mathbf{h}(t, \mathbf{r}_{PF}, \mathbf{v}_{PF}, \hat{\mathbf{y}}). \tag{4}$$

The estimation can be performed with the weighted non-linear least-squares method. To do so, on each iteration the problem is linearised around the current value of the estimated parameters, $\hat{\mathbf{y}}$, and the corresponding correction, $\Delta\hat{\mathbf{y}}$, is obtained by solving

$$\left(\mathbf{H}^T\mathbf{W}\mathbf{H}\right)\Delta\hat{\mathbf{y}} = \left(\mathbf{H}^T\mathbf{W}\right)\Delta\hat{\mathbf{z}}, \tag{5}$$

where $\mathbf{H}$ is the Jacobian, i.e., partials of the observations with respect to the estimated parameters, and $\Delta\hat{\mathbf{z}}$ is the difference between the actual and predicted observations. The Jacobian includes the state transition and sensitivity matrices of SGP4, which can be obtained numerically, as well as the partial derivatives of the measurements with respect to the state. Note that this corresponds to the classical orbit determination problem [27] but on a different set of estimated parameters and observations.

By solving the set of estimation problems, one for each fragment in the TLE catalogue, a distribution of $\Delta\mathbf{v}$ of the fragments can be inferred. The accuracy of SGP4 is limited and the propagation time, $t - t_F$ in Equation 4 ranges from weeks to months (see Figure 1). However, the main purpose of this approach is not to achieve a realistic characterisation of the $\Delta\mathbf{v}$ distribution, unfeasible due to SGP4, but to obtain a representative enough trend in terms of order of magnitude and dispersion.

2.1.2 NASA Standard Break-up Model

Although the previous approach provides the state (position and velocity) of each fragment, the corresponding size remains unknown. Besides, since it relies on TLE data available in SpaceTrack [1], it does not include fragments that have not been published, e.g., because they were not catalogued or properly tracked by 18^{th} SDS. In fact, the two weeks delay (see Figure 1 in Section 1) suggests the existence of this population gap, very likely related to very low and re-entering fragments.

To mitigate and also study these issues, the NASA SBM [12] has been used to simulate the size, area-to-mass ratio, A/m, and $\Delta\mathbf{v}$ of the fragments originated from the parent object. To do so, the position and velocity of the parent were taken from Equation 1 and the physical properties: mass, $m = 2180.38\,kg$ and area, $A = 13.217m^2$, from Database and Information System Characterising Objects in Space (DISCOS) [28]. The NASA SBM was used in explosion mode instead of the one for collisions given the unavailability of the interceptor's orbit. Additionally, it has been configured with a scaling factor, $S = 1$, and a minimum size of the fragments, $L_c = 1cm$, resulting in a total of 9,170 objects.

The $\Delta\mathbf{v}$ distribution of the fragments obtained with NASA SBM is shown in Figure 4, together with the one obtained from TLE data. Note that the histograms are normalised such that the integrals are equal to enable the comparison between the two populations, which have different number of fragments, and the lines represent the Cummulative Distribution Function (CDF). The three components of the $\Delta\mathbf{v}$ in the local RIC frame (radial, in-track and cross-track directions, with respect to the parent object state) are presented in Figure 4 (left) while the $\Delta\mathbf{v}$ magnitude in Figure 4 (right). Although the matching is not perfect, the $\Delta\mathbf{v}$ distributions from NASA SBM closely resemble those inferred with TLE data. Besides, there is matching in terms of order of magnitude and shape to COMSPOC analysis [25]. This agreement between NASA SBM and Cosmos 1408 ASAT test has been also confirmed by NASA [29].

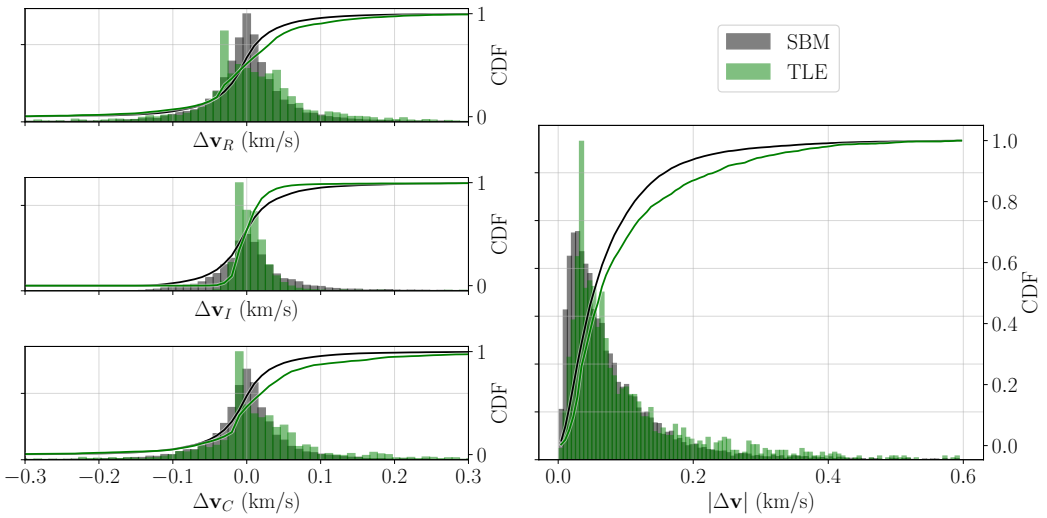

Figure 4: Distribution of $\Delta\mathbf{v}$ components in the RIC frame (left) and $\Delta\mathbf{v}$ magnitude (right) according to NASA SBM (black) and TLE data (green).

The Gabbard diagram of the simulated fragmentation is shown in Figure 5. Since the parent object is describing a nearly circular orbit before the impact, there is a clear intersection point (corresponding to the orbit of the parent object, with nearly same perigee and apogee heights) and the in-track and along-track components of the velocity are almost the same. Accordingly, Δv_I is directly related with changes in the orbital energy and thus, in the orbital period. Therefore, the points lying to the right of the vertical dotted line represent fragments with posigrade impulses ($\Delta v_I > 0$), while those lying to the left represent fragments with retrograde impulses ($\Delta v_I < 0$). Besides, due to the nearly circular orbit of the parent, the typical inclined X shape [30] is present. However, since the impulse has also some radial component (Δv_R), there are points lying outside the two main straight lines (above apogee and below perigee). Moreover, the angle between the two intersecting lines (slopes of the apogee and perigee lines) is related to the true anomaly of the parent object at the fragmentation epoch. Note the Gabbard diagram does not depend on ΔV_C since it is a velocity component out of the orbital plane, and not related to apogee, perigee nor orbital period. As in the $\Delta\mathbf{v}$ distribution, although the two sets of points in the Gabbard diagram do not match exactly, the agreement is noticeable. The plot matches the few available published Gabbard diagrams from SpaceNav [31], COMSPOC [25] and LeoLabs [32]. Finally, there is a clear gap in the fragments population from TLE data in the region below 92 min of orbital period, which corresponds to very low altitude fragments that may have reentered during the first weeks after the break-up event and therefore are not present in SpaceTrack [1].

Given the good agreement between the fragments inferred from TLE data and NASA SBM, we decided to use the latter because of the more complete distribution, not limited by 18$^{\text{th}}$ SDS operations and data publication procedures.

2.2 Observation simulation

Once the distribution of fragments at the break-up event epoch was obtained, the orbits of these fragments, taken as ground truth, were propagated further in time with a high fidelity numerical propagator: 30x30 EIGEN-6S2 gravity field, Sun and Moon third body perturbations with JPL DE405 ephemerides, NRLMSISE-00 atmosphere model and cannonball model for the Solar Radiation Pressure (SRP). The initial position is the same as the parent object, $\mathbf{r}_{PF}$, and the initial velocity is the one of the parent object plus the corresponding velocity increase as derived with NASA SBM, $\mathbf{v}_{PF} + \Delta\mathbf{v}$. The area and mass are taken from NASA SBM and the drag and SRP coefficients, C_D and C_R, respectively, are set to $C_D = 2$ and $C_R = 1$.

Then, observations during the first two weeks after the break-up event are simulated for an European ground-based radar survey network consisting of 3 stations located in Spain (*RSPA*), France (*RFRA*) and Germany (*RGER*) (see Figure 6). The field of view of the three sensors is modelled as conical with zenith pointing and 75 deg aperture (full angle). The power of the three sensors is also the same and corresponds to the Spanish Space Surveillance and Tracking Surveillance Radar (S3TSR) planned upgrade in 2028, with a minimum detectable target Radar Cross

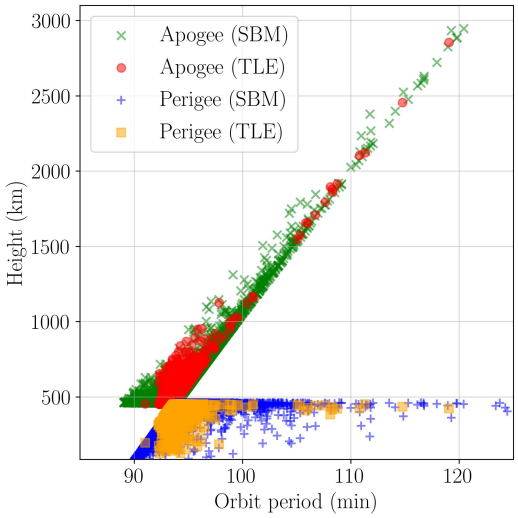

Figure 5: Gabbard diagram of the fragments from NASA SBM (crosses and pluses) and TLE data (filled circles and squares).

Section (RCS) of 0.012 m^2 at 1000 km distance [5]. These sensor network properties result in a total of 29,003 tracks from 1,644 observable objects, i.e., objects with at least one track. Figure 7 presents the distribution of the size of the fragments in a histogram together with the number of tracks available from each sensor for each size bin. Note that most of the fragments simulated with the NASA SBM are not observable due to minimum observable size constraints and there are many of them with a limited number of tracks available (see Figure 8). The observation spacing was set to 8 s, which results in a varying number of observations per track. The median track duration is of 72 seconds (9 observations per track, 1.63% of the orbital period of the parent object) and the distribution is presented in Figure 9. Since 4 tracks are usually required to initialise the orbit of a fragment in the catalogue, not every observable fragment is catalogable. A total of 1,182 fragments have at least 4 tracks and thus are considered detectable. Tracks from non-catalogable fragments (2.63%) have not been removed from the simulated data set as they represent clutter and contribute to provide a more realistic cataloguing campaign. The observations of each track contains a pair of angles (azimuth and elevation), range and range-rate with a 1-sigma measurement noise of 300 mdeg, 10 m and 1 m/s, respectively.

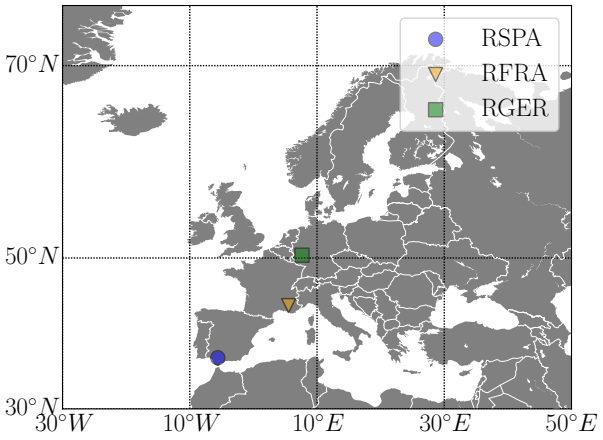

Figure 6: Location of the ground-based radar sensor network.

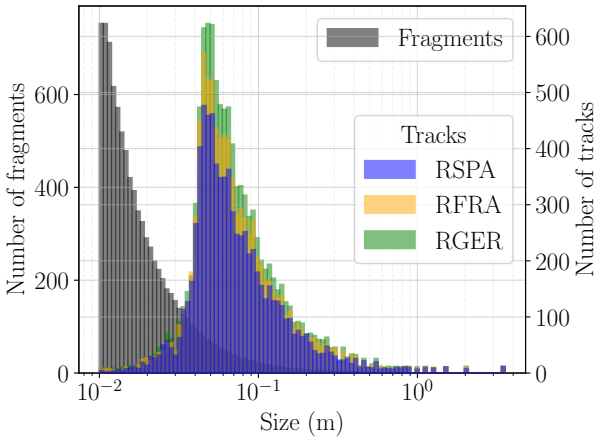

Figure 7: Distribution of size in terms of objects (black) and in terms of tracks from the different sensors (blue, orange and green).

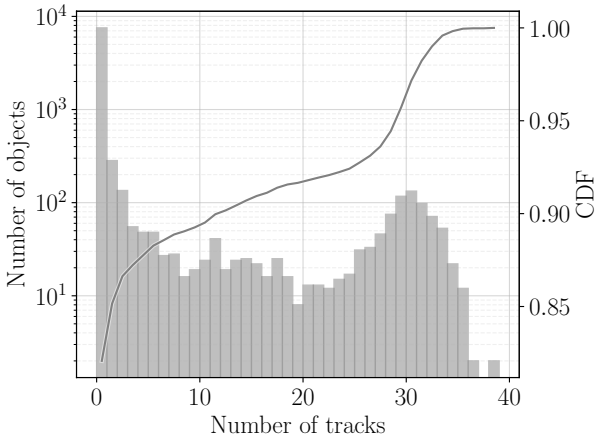

Figure 8: Distribution of the number of tracks per object.

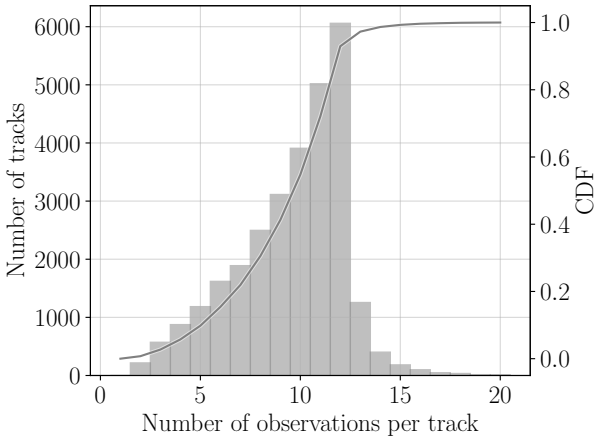

Figure 9: Distribution of the number of observations per track.

2.3 Cataloguing process

The cataloguing process is in charge of ingesting tracks, simulated as described above, to perform the build-up and maintenance of a catalogue of objects from the break-up event. Figure 10 depicts the overall process.

Since the focus of the study is on survey observations, the object tagging of each track is removed, so that we have UCTs, i.e., the fragment each track belongs to is unknown. Therefore, the first task to be carried out with each track is to correlate it with the existing catalogue through track-to-orbit correlation, also known as *track correlation*, to identify the fragment to which a track corresponds [33]. In case of successful correlation, the correlated track is used to perform orbit determination. In this task, the tracks are used to estimate an improved orbit of the fragment via batch estimation. Note that if no tracks are received for a catalogued fragment, then the trajectory description relies on orbit propagation. All these tasks are part of the maintenance of the catalogue.

In case a track is not correlated to any existing fragment in the catalogue, then it needs to go through track-to-track association, also known as *track association*. This methodology relies on a multi-target multi-sensor hypotheses-based method that is able to group tracks from common objects. A hypothesis is an association of certain number tracks assumed to have been originated from a common object. Hypotheses are first generated, then scored with a figure of merit based on the differences between the actual and a posteriori computed observations, pruned if it is proven that they are false and finally promoted whenever there is enough information (i.e., enough tracks) and the figure of merit is such that the associated tracks are expected to belong to the same fragment. See [34] for a full description of this track association methodology. The need for track association arises from the fact that a single track does not normally contain enough information to initialise a fragment from one track in the catalogue with an orbit of sufficient accuracy to allow the correlation of further tracks [35]. Thus, it is normally required to associate at least four tracks together to estimate the orbit of a new object and add it to the catalogue with enough accuracy [35]. This track association process relies considerably on Initial Orbit Determination (IOD) algorithms [36] in order to compute orbits from tracks without any a priori information. Once an accurate orbit has been obtained, a new object is added to the catalogue.

2.4 Fragmentation analysis

The catalogued orbits can be used to estimate the fragmentation epoch, t_F. This point can be approximated as a pinch point at which all the fragments have the same position but different velocity. Therefore, this means that the dispersion of the position vectors of the catalogued objects of the cloud is expected to be minimum at t_F. The fragments then spread along different orbits through time, thus increasing their dispersion.

The first reliable orbit estimation of a certain fragment is available as soon as a hypothesis containing the tracks from this fragment is promoted via track association. Although this may happen several days after fragmentation, this first estimated state can be propagated backwards in time, thus obtaining an estimation of the position trajectory of each fragment. The dispersion of N fragments in the i^{th} direction can be characterised by the standard deviation, i.e.,

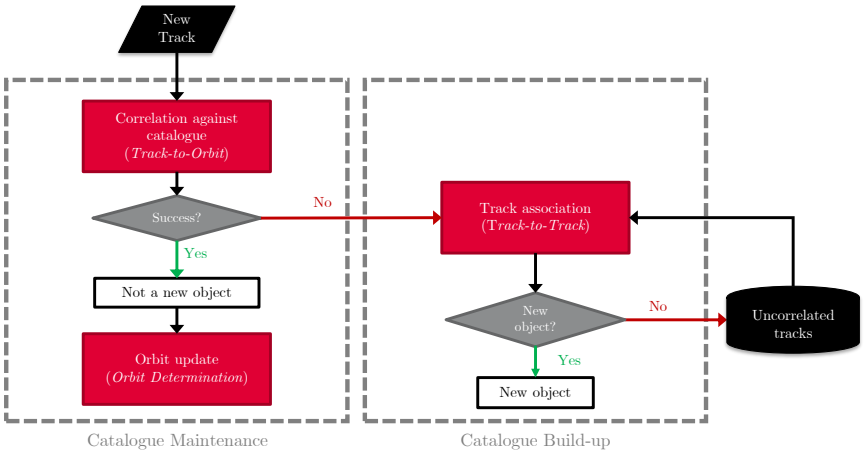

Figure 10: Cataloguing chain.

$$\sigma_{r_i}(t) = \sqrt{\frac{1}{N}\sum_{j}^{N}\left[\hat{\mathbf{r}}_{i,j}(t) - \bar{\hat{\mathbf{r}}}_i(t)\right]^2}, \tag{6}$$

where $\hat{\mathbf{r}}_{i,j}(t)$ is the i^{th} component of the estimated position at epoch t of the j^{th} object and $\bar{\hat{\mathbf{r}}}_i(t)$ is the corresponding mean value. Then, it is possible to condense the three components into a single scalar, by defining a global dispersion as:

$$\zeta(t) = \sqrt{\frac{1}{3}\sum_{i}^{3}\sigma_{r_i}^2(t)}. \tag{7}$$

Therefore, the fragmentation epoch can be estimated as the one at which $\zeta(t)$ is minimum.

Besides, the fact that the dispersion is minimum at the fragmentation epoch can also be used to identify false positives during track association. Once the fragmentation epoch is estimated, the distribution of estimated positions at this point can be analysed to identify outliers, i.e., spurious objects that do not correspond to any fragment from the break-up event.

A simple outlier rejection process is proposed here to filter out false positive track association hypotheses. First, locate the hypothesis J and the direction I such that the distance of the estimated position value at $\hat{t}_F$ to the mean value normalised with the standard deviation is maximum, i.e.,:

$$\exists I, J : \frac{\left|\hat{r}_{I,J}(\hat{t}_F) - \bar{\hat{r}}_I(\hat{t}_F)\right|}{\sigma_{r_I}(\hat{t}_F)} > \frac{\left|\hat{r}_{I,j}(\hat{t}_F) - \bar{\hat{r}}_I(\hat{t}_F)\right|}{\sigma_{r_I}(\hat{t}_F)} \quad \forall j \neq J. \tag{8}$$

This hypothesis J represents an outlier candidate because its dispersion on direction I is maximum over the complete data set. Then, two additional conditions must be fulfilled to confirm the outlier:

$$\exists I : \begin{cases} \left|\hat{r}_{I,J}(\hat{t}_F) - \bar{\hat{r}}_I(\hat{t}_F)\right| > \alpha\sigma_{r_I}(\hat{t}_F) \\ \beta\sigma_{r_I}(\hat{t}_F) > \sigma_{r_{I0}}(\hat{t}_F) \end{cases}, \tag{9}$$

being $\sigma_{r_{I0}}(\hat{t}_F)$ the initial (before outlier rejection) standard deviation over direction I, and α and β two threshold parameters. If no direction I is found from Equation 9 then the outlier rejection process is stopped. Otherwise, hypothesis J is removed and a new candidate hypothesis is selected with Equation 8. Note that the outlier rejection strategy requires the false positives to be outliers per se, this is, enough true positives are required to capture the fragmentation epoch and a reliable enough value for $\bar{\hat{\mathbf{r}}}_i(t)$.

3. RESULTS

The outcomes from the cataloguing sequence introduced in Section 2.3 using the tracks generated as described in Section 2.2 for the fragmentation cloud simulated in Section 2.1 are presented and discussed in this section. Firstly, catalogue build-up is tackled, including track association, fragmentation epoch estimation and false positive outlier rejection. Secondly, catalogue maintenance is addressed, including track correlation, evolution of false positives and orbit accuracy. A total of 29,003 UCTs corresponding to the first two weeks after the Cosmos 1408 ASAT test (from 2021-11-15T04:30 to 2021-11-29T02:45) comprise the input data-set. The cataloguing process starts from an empty catalogue and any a priori information is used.

3.1 Catalogue build-up

The track association is the main player during the cataloguing build-up, as it drives the process during the first days after the fragmentation event. As soon as UCTs are received, new hypotheses are generated, resulting in what is known as growth of the hypotheses tree. This growth goes on until some of the hypotheses are promoted, i.e., new objects added to the catalogue, because the promotion also implies the invalidation of incompatible hypotheses under the assumption that a single track cannot belong to more than one object. Thanks to this pruning of the hypotheses tree, it is possible to alleviate the track association procedure, reduce the computational burden and keep the problem solvable from a real-time operational perspective. Besides, once the catalogue is populated with the orbits of the fragments, the track correlation starts correlating UCTs with already catalogued and maintained orbits, reducing the track association burden. Figure 11 shows the evolution of the number of non-promoted and promoted hypotheses. Note that the number of non-promoted hypotheses does not decrease further from 23rd Nov because old hypotheses have not been removed for analysis purposes. In an operational scenario, hypotheses whose last associated track is older than certain time period, e.g., two weeks, should be pruned.

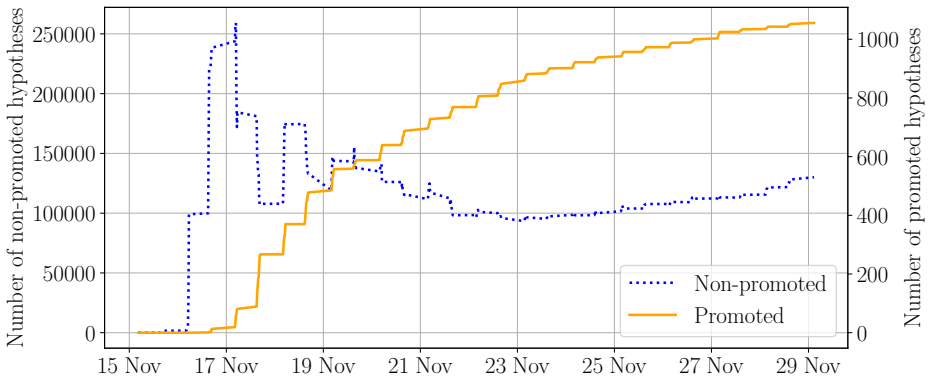

Figure 11: Evolution of the number of non-promoted hypotheses (blue) and promoted hypotheses (orange) along time.

As stated in Section 2.3, 4 tracks are required to promote a hypothesis during track association and then initialise the orbit of a new fragment in the catalogue. Figure 12 shows the distribution of the figure of merit of hypotheses of 2 (left) and 3 (right) tracks as a function of the time span between the first and last associated tracks at the end of the cataloguing process. Blue pluses and purple triangles represent, respectively, true negatives (i.e., non-promoted hypotheses containing tracks from different fragments) and false negatives (i.e., non-promoted hypotheses containing tracks from the same fragment). Despite of the different distributions of figure of merit of true and false negatives of 2 tracks (see right histograms), they are overlapping, what prevents threshold gating. This is also the case for true and false negatives of 3 tracks, although true negatives start to concentrate in higher figure of merit values. Regarding the distribution over the time span between the first and last associated tracks, the hypotheses concentrate in low time span region (below 5 days) due to the mismatching between the dynamical model of the ground truth and that of the track association. As the time between the tracks to be associated increases, the association becomes more challenging. Note that the time span between the associated tracks is not per se related to the physical time, i.e., hypotheses with low time span are not necessarily related to tracks from the first days after the fragmentation. However, as tracks are correlated when the corresponding fragment has been catalogued, a higher density of hypotheses in the first days is expected, when the fragments have not been already catalogued.

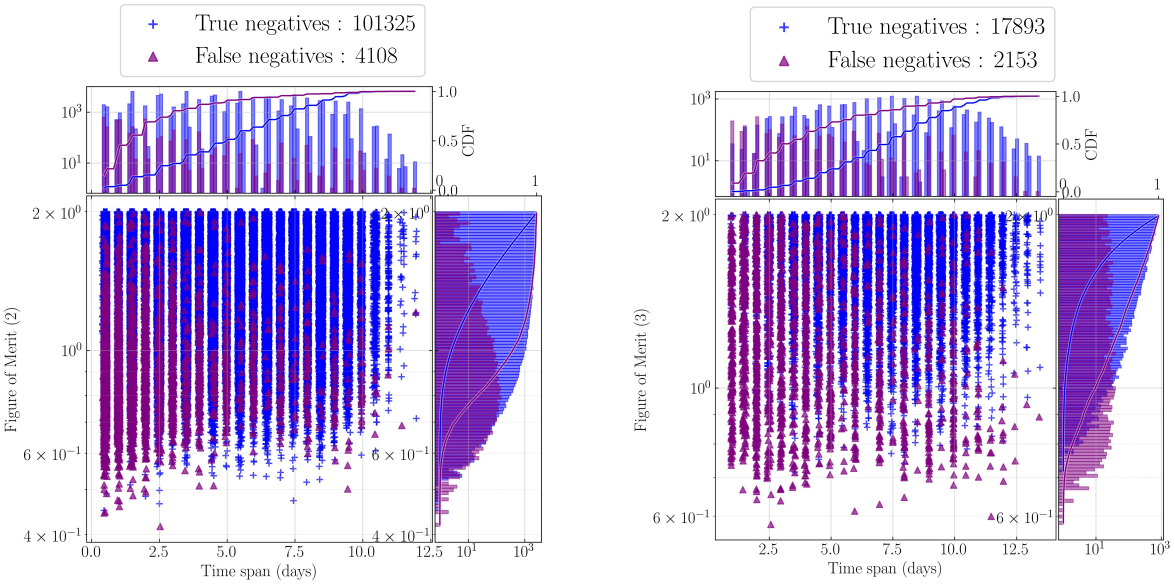

Figure 12: Distribution of the figure of merit of track association hypotheses of 2 tracks (left) and 3 tracks (right) as a function of the time span between first and last associated tracks at the end of the cataloguing process.

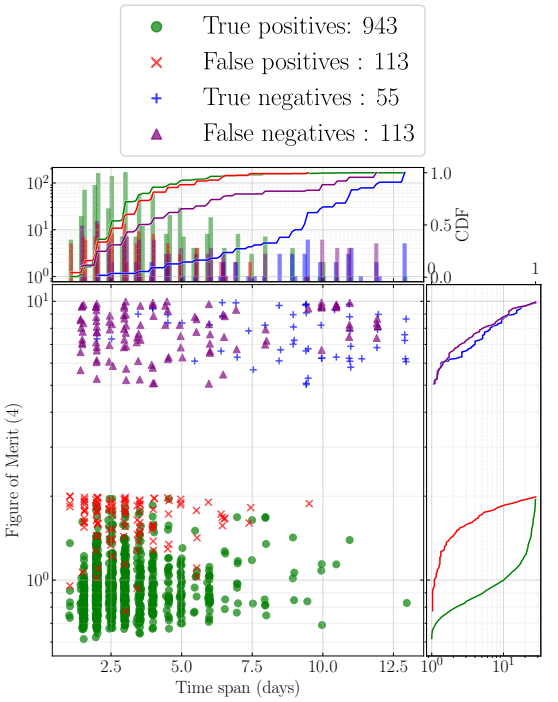

Figure 13: Distribution of the figure of merit of track association hypotheses of 4 tracks as a function of the time span between first and last associated tracks at the end of the cataloguing process.

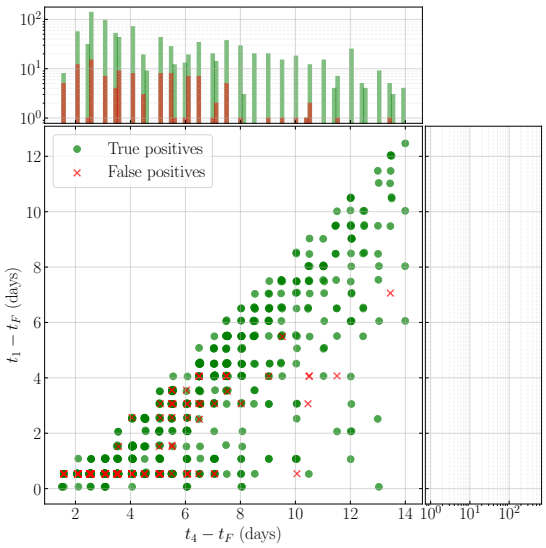

Figure 14: Distribution of the first and last associated track epoch (t_1 and t_4, respectively) of promoted hypotheses.

Analogously, Figure 13 shows the distribution of the figure of merit of hypotheses of 4 tracks as a function of the time span between the first and last associated tracks at the end of the cataloguing process. In this case, since hypotheses of 4 tracks can be promoted, we have also true positives (i.e., promoted hypotheses containing tracks from the same fragment) and false positives (i.e., promoted hypotheses containing tracks from different fragments), which are depicted with green circles and red crosses, respectively. The gap between positives and negatives is just a consequence of the promotion step and the gating process. Besides, the figure of merit distributions of true and false positives do not overlap as much as true and false negatives of hypotheses of 2 and 3 tracks. In fact, it is this what enables the threshold gating during promotion.

At first sight, the number of false positives may seem too high, 113 of the total of 1,056 promoted hypotheses, i.e. 10.7%. However, the concept of false positive should be handled with care in fragmentation scenarios. Just after the fragmentation epoch, t_F, the fragments are so close to the pinch point that some of them could be even indistinguishable, as not enough time has elapsed for them to spread along the orbit space. Therefore, hypotheses containing tracks received on the first hours after the event are expected to pose great challenges to the catalogue build-up process. To support this, Figure 14 presents the distribution of the promoted hypotheses (true positives and false positives) in the plane of the first and last associated tracks, t_1 and t_4, respectively. Most of the false positives (76 out of 113, i.e., 67.25%) have as first associated track, one from within the first 15 hours. There are 59 (52.21%) false positives involving 2 fragments, 31 (27.43%) involving 3 fragments and 23 (20.35%) involving 4 fragments. As it will be discussed in Section 3.2, most of the false positives do not imply a major pollution of the catalogue.

The lower the number of tracks available for a fragment, the more challenging the cataloguing is. This is confirmed in Figure 15, where the distribution of the number of tracks of for each fragment simulated (grey) and catalogued (green) is showcased. Most of the non-catalogued fragments have a low number of tracks. Observability conditions and the track association process itself prevent these fragments from being catalogued.

The fragmentation epoch has been estimated as discussed in Section 2.4, considering every promoted hypothesis during track association and its corresponding estimation propagated backwards. Figure 16 presents the dispersion of these trajectories, σ_{r_i} and the global dispersion, ζ, along time. It is clear how the minimum of all dispersion metrics is reached at the true fragmentation epoch, depicted as a vertical red dotted line. In fact, the estimated fragmentation epoch is $\hat{t}_F =$ 2021-11-15T02:46, two minutes earlier than the true value.

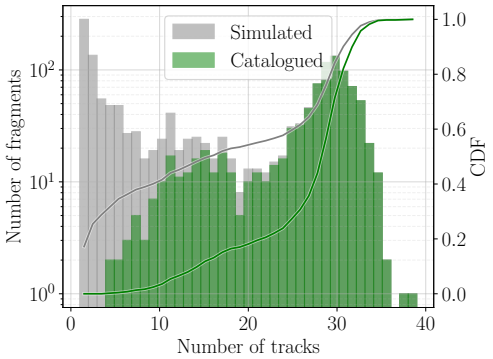

Figure 15: Distribution of the number of tracks per simulated (grey) and catalogued (green) fragment.

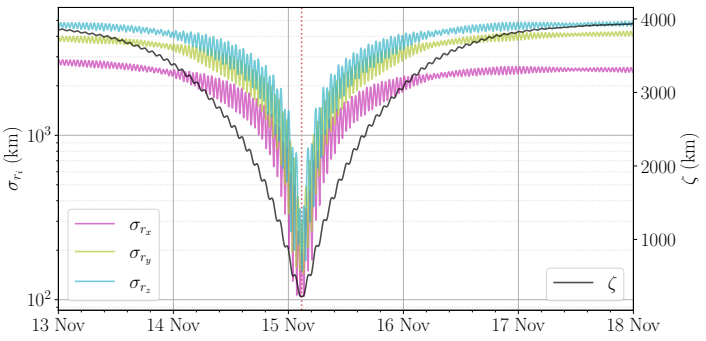

Figure 16: Evolution of the position dispersion trough time.

Moreover, the false positive outlier rejection method presented in Section 2.4 has been applied with $\alpha = 5$ and $\beta = 20$. The distribution of the position dispersion at $\hat{t}_F$ of the promoted hypotheses during track association before the outlier rejection is presented in Figure 17 (top). It includes a breakdown by number of fragments involved and the hypotheses are the same as in Figure 13. Note how false positives tend to distribute over the tails of the distributions. On the contrary, Figure 17 (bottom) shows the remaining hypotheses after the outlier rejection. The proposed outlier rejection reduces the total number number of false positives from 113 to 50, i.e. almost a 56% of the total number of false positives, while only 2 true positives (0.2%) have been wrongly filtered out as outliers. These two hypotheses were the 1018$^{\text{th}}$ and 994$^{\text{th}}$, promoted on 27$^{\text{th}}$ and 26$^{\text{th}}$ Nov, respectively, thus requiring a long propagation interval down to the fragmentation epoch. The major reduction of false positives is related to those involving 3 and 4 tracks, since

those involving 2 tracks, as discussed in Section 3.1 may involve a pair of fragments indistinguishable just after the fragmentation. The number of false positives involving 2 tracks is reduced just a 31%, from 59 to 41, while those of 3 and 4 tracks are reduced 81% and 87%, from 31 to 6 and from 23 to 3, respectively.

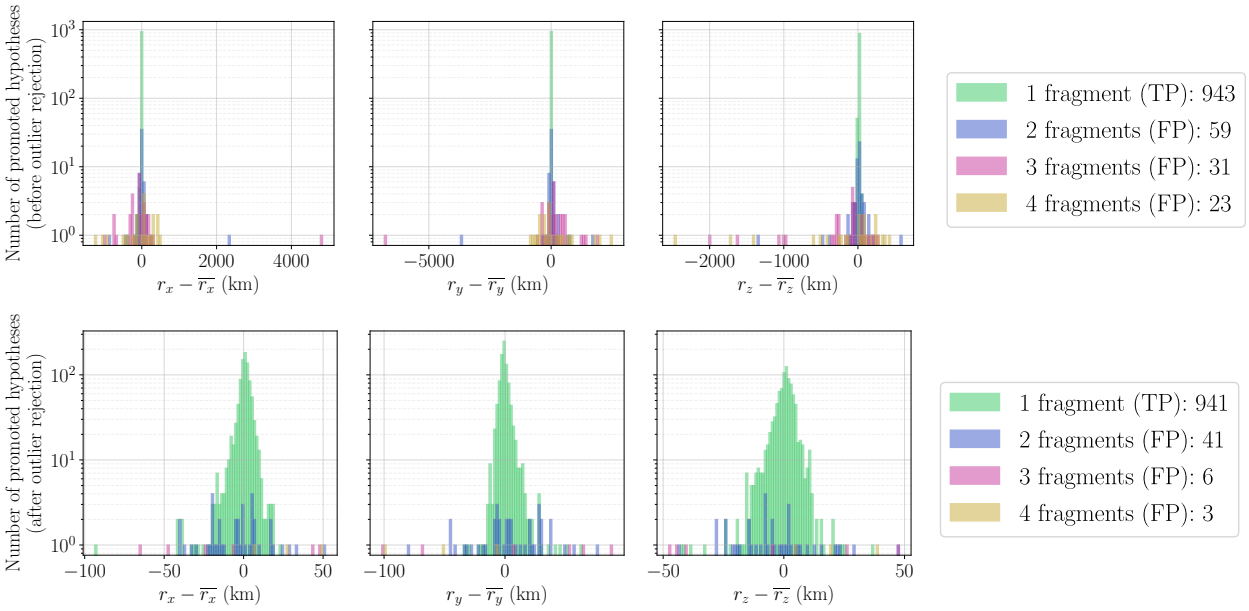

Figure 17: Distribution of the position dispersion at the estimated fragmentation epoch of each promoted hypothesis before (top) and after (bottom) outlier rejection.

3.2 Catalogue maintenance

The track correlation starts driving the cataloguing maintenance as soon as the catalogue is filled with the catalogued fragments. Figure 18 shows the distribution of the weighted Root Mean Square (RMS) of the observation residuals between UCTs and predicted observations from catalogued orbits, as a function of time since the fragmentation. Note that although the track correlation is performed by evaluating and gating the weighted RMS for the four types of measurements (azimuth, elevation, range and range-rate), the total weighted RMS is presented instead as it exhibits a global and representative behaviour. There are no pairs before the second day because the first catalogued fragments are created by the track association after around 1.5-2 days from the fragmentation epoch (see Figure 14) and the following observation window happens after the second day.

There is a clear separation between true and false pairs, which enables an efficient gating of false pairs. From the tracks that are correlated, only 0.11% of them are wrongly correlated (false positives). Note that there is only 15 false positives, 13 of which are inherited from the track association. Besides, the rate of false negatives is 5.24% (with respect to the sum true positives and false negatives).

The number and impact of the false positives during track correlation has been analysed together with track associations ones. Figure 19 provides a summary of the origin of true and false positives during track association and correlation. Firstly, note that some of the true positives from track association lead to false positives in track correlation. Nevertheless, they are only 13 tracks from 13 different objects, thus not jeopardising the reliability of the catalogue. They correspond to cases in which only one track is wrongly associated to the object, so the impact on the orbit estimation is negligible. Secondly, note that a track correlated with a false positive from track association is considered as true positive if three of the four tracks associated by track association belong to the same fragment as this correlated track. This is another evidence of the low impact of track association false positives involving only two fragments. This is the case of 17% (19) of the false hypotheses promoted during track association. However, these objects are updated with correlated tracks, all belonging to the same fragment (the same as three of the four associated tracks). The rest of the false hypotheses promoted during track association, 83% (94), do not correlate with any future tracks, i.e., those objects are not maintained and thus could be considered as dead or spurious objects. This explains why false positives from the track association are not polluting noticeably the catalogue. Finally, there are 2

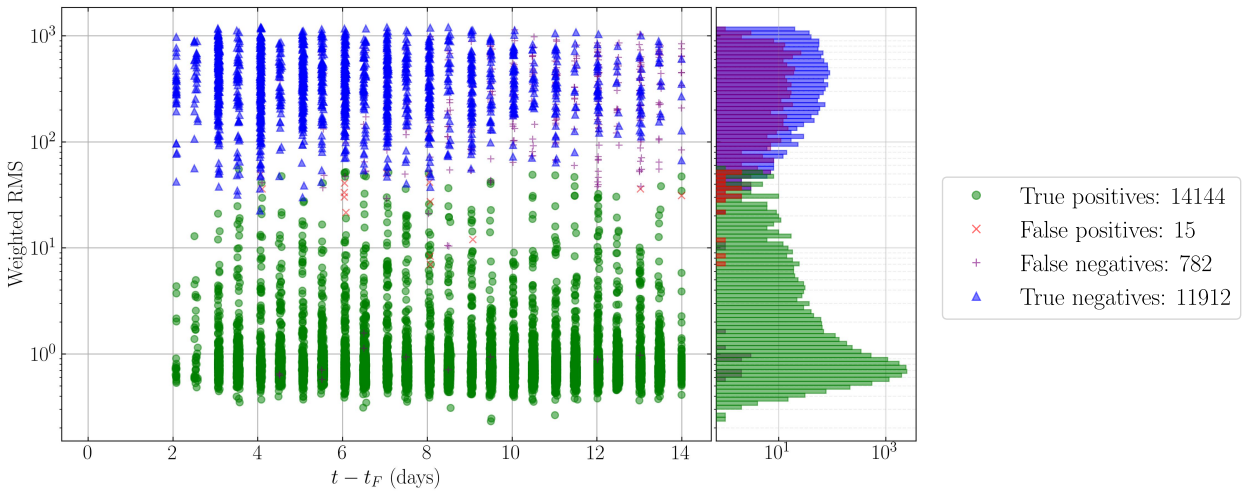

Figure 18: Distribution of weighted RMS in track correlation as a function of the time of the track from the fragmentation epoch.

tracks related to track association false positives: 1) the orbit from a track association of the type BACA correlated with a track from A, and 2) the orbit from a track association of the type BBAA correlated with a track from A.

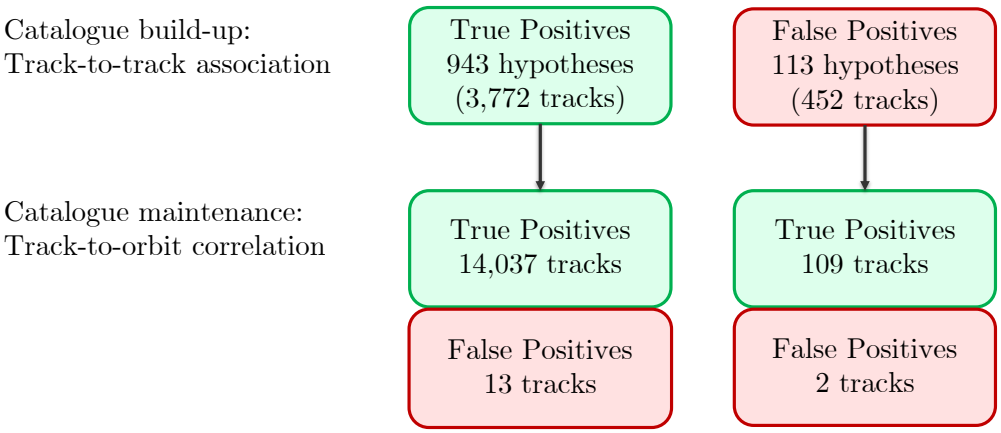

Figure 19: Breakdown of the true and false positives along the track association (catalogue build-up) and track correlation (catalogue maintenance).

Finally, Figure 20 shows the position error of the maintained orbits of the catalogued objects after two weeks of simulation in the local RIC frame (i.e., differences with respect to the orbits of the simulated population of fragments). Each sample of the distribution corresponds to the RMS of the differences of the position components between the estimated orbit and the ground truth during one orbital period after the last used observation. As expected, the direction with higher error is the in-track, since it is perpendicular to the position vector and almost aligned with the velocity vector, which is the main direction of the motion. Although there are some objects with differences of the order of the kilometre, most of them are located around the 10 metres in the in-track direction.

4. CONCLUSIONS

This paper analysed the catalogue build-up and maintenance process in a simulated scenario of the Cosmos 1408 ASAT test that took place on 15th November 2021. Starting from scratch and without any a priori information, the operational build-up and maintenance of a catalogue have been studied with a sensor network of three survey radars

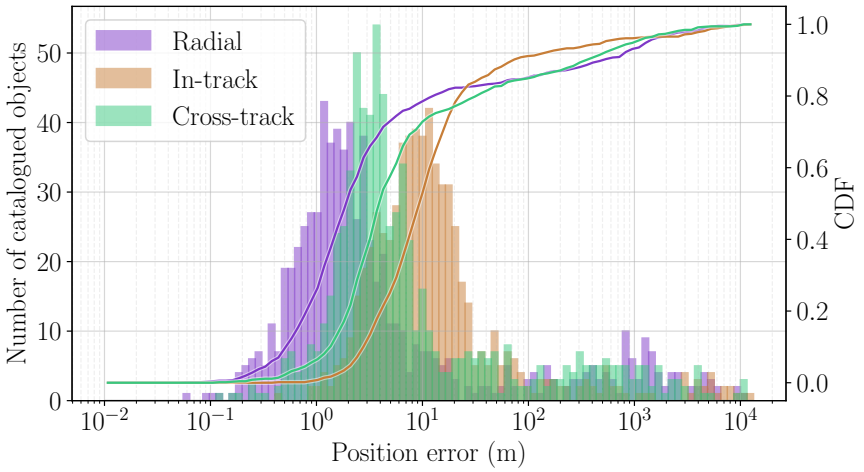

Figure 20: Distribution of position errors in the local RIC frame of the catalogued orbits after the two weeks.

located in Europe. The proposed methodology is suitable for early identification and tracking of fragments from such events. The first day after the fragmentation the track association starts populating the catalogue and adding more and more fragments as soon as tracks are received and fragments spread along the orbit.

The authors hope that this work helps to improve the time taken by operators and operations centres on identifying and tracking the fragments after these events so that the provision of SSA and STM products can be maintained. It has been shown how long blackouts, such as the two weeks blackout in SpaceTrack [1], can be reduced by using robust, efficient and automated methods for track association and track correlation within the cataloguing process. This is particularly relevant for highly congested regions, such as LEO, where the Cosmos 1408 ASAT test happened, and a population of untracked fragments may increase the collision risk with neighbour objects.

Future work will tackle the identification of duplicated objects in the catalogue, by the use of orbit-to-orbit correlation methods [33]. Besides, we will investigate the detection of ambiguities during track association and the use of more than four tracks in those cases.

ACKNOWLEDGEMENTS

This project has received funding from the “Comunidad de Madrid” under “Ayudas destinadas a la realización de doctorados industriales” program (project IND2017/TIC7700).

Besides, the authors would like to acknowledge Alfredo Antón for providing the implementation of the NASA SBM.

REFERENCES

[1] 18th Space Control Squadron, Space-Track, [Online; last accessed 1-Aug-2022] (2022).
URL `https://www.space-track.org`

[2] T. Kelso, CelesTrak, [Online; last accessed 1-Aug-2022] (2022).
URL `https://celestrak.org`

[3] P. Anz-Meador, J. Opiela, D. Shoots, J. Liou, History of on-orbit satellite fragmentations, 15th edition, Tech. Rep. NASA/TM–2018–220037, NASA Orbital Debris Program Office (2018).

[4] H. Klinkrad, Space Debris: Models and Risk Analysis, Springer-Verlag Berlin Heidelberg, 2006. `doi:10.1007/3-540-37674-7`.

[5] J. Siminski, D. Cano Mañanes, M. Alessandrini, C. Pérez Hernández, G. Pinna, P.-M. Besso, J. Rey Benayas, S. Rodríguez Rodríguez, G. Ojeda Rodríguez, P. Íñiguez Cano, C. Lluch Jouyd, J. Martínez-Villa Salmerón, Research and performance analysis of the spanish surveillance radar, in: 72th International Astronautical Congress, 2021.

[6] ESA Space Debris Office, ESA's Annual Space Environment Report, Tech. Rep. GEN-DB-LOG-00288-OPS-SD, ESA Space Debris Office (Apr. 2022).
URL https://www.sdo.esoc.esa.int/environment_report/Space_Environment_Report_latest.pdf

[7] R. Crowther, R. Walker, J. Dick, S. Green, J. Marchant, Detectability of satellite fragmentations in highly eccentric orbits, Master's thesis (jan 1995). doi:10.1016/0273-1177(95)98762-d.

[8] N. Johnson, The cause and consequences of a satellite fragmentation: A case study, Advances in Space Research 23 (1) (1999) 165–173. doi:10.1016/s0273-1177(98)00243-9.

[9] L. Anselmo, C. Pardini, The effects of spacecraft and upper stage breakups on the geostationary ring, Tech. rep., Consiglio Nazionale delle Ricerche (2000).

[10] C. Saunders, Modelling of the optical observations of a geosynchronous fragmentation event, Acta Astronautica 60 (8-9) (2007) 752–762. doi:10.1016/j.actaastro.2006.07.021.

[11] T. Schildknecht, A. Vananti, E. Cordelli, T. Flohrer, ESA optical surveys to characterize recent fragmentation events in GEO and HEO, in: S. Ryan (Ed.), Advanced Maui Optical and Space Surveillance Technologies Conference, 2019, p. 34.

[12] N. Johnson, P. Krisko, J.-C. Liou, P. Anz-Meador, Nasa's new breakup model of evolve 4.0, Advances in Space Research 28 (9) (2001) 1377–1384. doi:10.1016/s0273-1177(01)00423-9.

[13] N. Singh, A. Poore, C. Sheaff, J. Aristoff, M. Jah, Multiple Hypothesis Tracking (MHT) for space surveillance: results and simulation studies, in: Advanced Maui Optical and Space Surveillance Technologies (AMOS) Conference, 2013, p. E16.
URL http://adsabs.harvard.edu/abs/2013amos.confE..16S

[14] V. Agapov, A. Lapshin, Survey and follow-up strategies used in operation of ASPOS OKP to gather observation data on GEO, HEO and MEO objects, in: T. Flohrer, R. Jehn, F. Schmitz (Eds.), 1st NEO and Debris Detection Conference, Vol. 8, ESA Space Safety Programme Office, 2019.

[15] G. Zarcone, L. Mariani, M. Rossetti, L. Cimino, S. H. Hossein, F. Piergentili, F. Santoni, F. Curianò, Optical observations for energetic characterization of in-orbit explosion: the FREGAT-SB case, in: T. Flohrer, S. Lemmens, F. Schmitz (Eds.), 8th European Conference on Space Debris, Vol. 8, ESA Space Debris Office, 2021.

[16] N. L. Johnson, E. Stansbery, J.-C. Liou, M. Horstman, C. Stokely, D. Whitlock, The characteristics and consequences of the break-up of the Fengyun-1C spacecraft, Acta Astronautica 63 (1-4) (2008) 128–135. doi:10.1016/j.actaastro.2007.12.044.

[17] K. Tetreault, S. D. Ross, K. Schroeder, J. Black, Fragmentation event identification using back propagation with variable ballistic coefficient calculation, in: Advanced Maui Optical and Space Surveillance Technologies Conference, 2018.

[18] A. Muciaccia, Fragmentations in low earth orbit: event detection and parent body identification, Master's thesis, Politecnico di Milano (2021).

[19] JSC "Vimpel Interstate Corporation" and the Keldysh Institute of Applied Mathematics (IAM), JSC Vimpel data portal (Accessed Aug 2021).
URL http://spacedata.vimpel.ru/

[20] P. Ravi, C. Frueh, T. Schildknecht, Investigation of three recent Atlas V Centaur upper stage fragmentation events, in: T. Flohrer, S. Lemmens, F. Schmitz (Eds.), 8th European Conference on Space Debris, Vol. 8, ESA Space Debris Office, 2021.

[21] W. Faber, W. Zaidi, J. Schumacher, Paul, Early blast point determination for large GEO fragmentation events, in: S. Ryan (Ed.), Advanced Maui Optical and Space Surveillance Technologies Conference, 2018, p. 22.

[22] L. Dimare, S. Cicalò, A. Rossi, E. M. Alessi, G. B. Valsecchi, In-orbit fragmentation characterization and parent bodies identification by means of orbital distances, in: First International Orbital Debris Conference, Vol. 2109, 2019, p. 6007.

[23] J. McDowell, Jonathan's Space Report - The 2021 Nudol' test, [Online; accessed 1-May-2022] (2022).
URL https://planet4589.org/space/asat/nudol.html

[24] EU SST, EU SST confirms the fragmentation of space object COSMOS 1408, [Online; accessed 1-May-2022] (2022).
URL https://www.eusst.eu/newsroom/eu-sst-confirms-fragmentation-cosmos-1408/

[25] D. Oltrogge, S. Alfano, D. Vallado, P. Zimmer, R. Hall, J. Wilson, M. Siegers, J. Aurich, Russian ASAT debris cloud evolution and risk, in: 3rd International Conference on Space Situational Awareness (ICSSA), 2022.

[26] D. Vallado, P. Crawford, R. Hujsak, T. S. Kelso, Revisiting spacetrack report #3: Rev 2, in: AIAA/AAS Astrodynamics Specialist Conference and Exhibit, American Institute of Aeronautics and Astronautics, 2006. doi:10.2514/6.2006-6753.

[27] O. Montenbruck, E. Gill, Satellite Orbits: Models, Methods and Applications, Springer-Verlag Berlin Heidelberg, 2000. doi:10.1007/978-3-642-58351-3.

[28] European Space Agency, (Database and Information System Characterising Objects in Space (DISCOS), [Online; accessed 1-May-2022] (2022).
URL https://www.space-track.org

[29] NASA Orbital Debris Program Office, Orbital Debris Quarterly News (Volume 26, Issue 1), March 2022, Tech. rep., National Aeronautics and Space Administration (Mar. 2022).

[30] A. Tan, R. C. Reynolds, Theory of satellite fragmentation in orbit, World Scientific Publishing Co. Pte. Ltd., 2020. doi:10.1142/11506.

[31] SpaceNav, Updated orbital element distribution from the COSMOS 1408 ASAT event, [20-Nov-2022] (2022).
URL https://twitter.com/SpaceNav2

[32] D. McKnight, M. Stevenson, M. Shouppe, J. Rowland, H. She, B. Reihs, Cosmos 1408 - Stress Test for LeoLabs, in: 3rd International Conference on Space Situational Awareness (ICSSA), 2022.

[33] A. Pastor, D. Escobar, A. Águeda, M. Sanjurjo, Data processing methods for catalogue build-up and maintenance, in: T. Flohrer, R. Jehn, F. Schmitz (Eds.), 1st NEO and Debris Detection Conference, Vol. 1, ESA Space Safety Programme Office, Darmstadt, Germany, 2019.
URL https://conference.sdo.esoc.esa.int/proceedings/neosst1/paper/468

[34] A. Pastor, M. Sanjurjo-Rivo, D. Escobar, Track-to-track association methodology for operational surveillance scenarios with radar observations, CEAS Space Journal (accepted for publication, CEAS-D-21-00122R1) (2022).

[35] K. Hill, C. Sabol, K. T. Alfriend, Comparison of covariance based track association approaches using simulated radar data, The Journal of the Astronautical Sciences 59 (1-2) (2012) 281–300. doi:10.1007/s40295-013-0018-1.

[36] A. Pastor, M. Sanjurjo-Rivo, D. Escobar, Initial orbit determination methods for track-to-track association, Advances in Space Research 68 (7) (2021) 2677–2694. doi:10.1016/j.asr.2021.06.042.